

Joint time-domain modelling magnetic field variations of ionospheric and magnetospheric origin. A concept and its implementation

Mikhail Kruglyakov (1) and Alexey Kuvshinov (2)

(1) University of Otago, Dunedin, New Zealand (mikhail.kruglyakov@otago.ac.nz)
(2) ETH Zurich, Switzerland (kuvshinov@erdw.ethz.ch)



1 Abstract

We present an approach to model the spatio-temporal evolution of magnetic fields due to magnetospheric and ionospheric sources simultaneously. An approach exploits two types of source parameterization (data-based and physics-based) and accounts for 3-D electromagnetic (EM) induction effects. Using observatory data, we obtain continuous spatio-temporal models of multi-source external and induced magnetic fields for the years 1998-2021. We also discuss an adaptation of the approach for the analysis of satellite data (like *Swarm* and *MSS*).

2 Motivation

Accurate global models of the spatial-temporal structure of external current systems are critical for probing the Earth's interior. Such models can also be helpful for better isolating core and crustal fields.

Three *ionospheric* current systems – equatorial electrojet (EEJ), polar electrojet (PEJ), and mid-latitude current system (MLCS; in quiet time called Sq) – produce quasi-periodic daily variations (DV). Of note: a) EEJ and PEJ have much smaller spatial structures than MLCS; b) EEJ and MLCS are *day-time* phenomenon.

Signals at longer periods (LP) are due to irregular fluctuations of *magnetospheric* ring current (RC), and their spatial morphology is usually approximated by the spherical harmonics (SH) of low degree and order.

Usually, DV and LP signals are treated *separately*. For example, the analysis of RC signals is often based on night-time data to diminish the effects from ionospheric sources. However, due to EM induction in the Earth, the signals of ionospheric origin also persist during the night [4]. As for DV, their analysis is usually performed in the *frequency domain* (FD). However, the morphology of all ionospheric sources varies from day to day, depending on the solar activity and the Earth's orbital position, advocating analysis of DV in time domain (TD). In addition, the analysis of EEJ and MLCS signals is based on non-polar data to diminish the effects from PEJ. But, this questions what is the non-polar data.

In this study, we extend a methodology presented in [6] to *simultaneously* model magnetic fields from all the sources discussed above *directly in the time domain* (TD) using *non-polar* and *polar* data. The methodology works with observatory and satellite data but is explained and implemented to observatory data.

3 Modelling (mostly) magnetospheric signals

We describe signals (which are primarily due to large-scale RC source) using SH parameterization. Note, that there are indications that part of these signals is of ionospheric origin. Following [6], these SH-parameterized signals at a given time instant can be written as

$$\mathbf{B}^{\text{mix,SH}}(\mathbf{r}, t_k; \sigma) = \sum_{l,m} \sum_{n=0}^{N_l} \mathcal{E}_l^m(t_k - n\Delta t) M_{\mathbf{B}_l^m}^n(\mathbf{r}, T; \sigma) \quad (1)$$

Here σ - Earth's conductivity (Fig. 1), $T = N_l \Delta t$ (T taken as half a year), $\Delta t = 1$ hour, $M_{\mathbf{B}_l^m}^n$: time-invariant weights; their calculation is discussed in Section 5, $\mathbf{r} = (r, \vartheta, \varphi)$, \mathcal{E}_l^m : external SH coefficients.

Superscript "mix" means that **with observatory data only, one cannot separate magnetospheric and ionospheric contributions to these signals.**

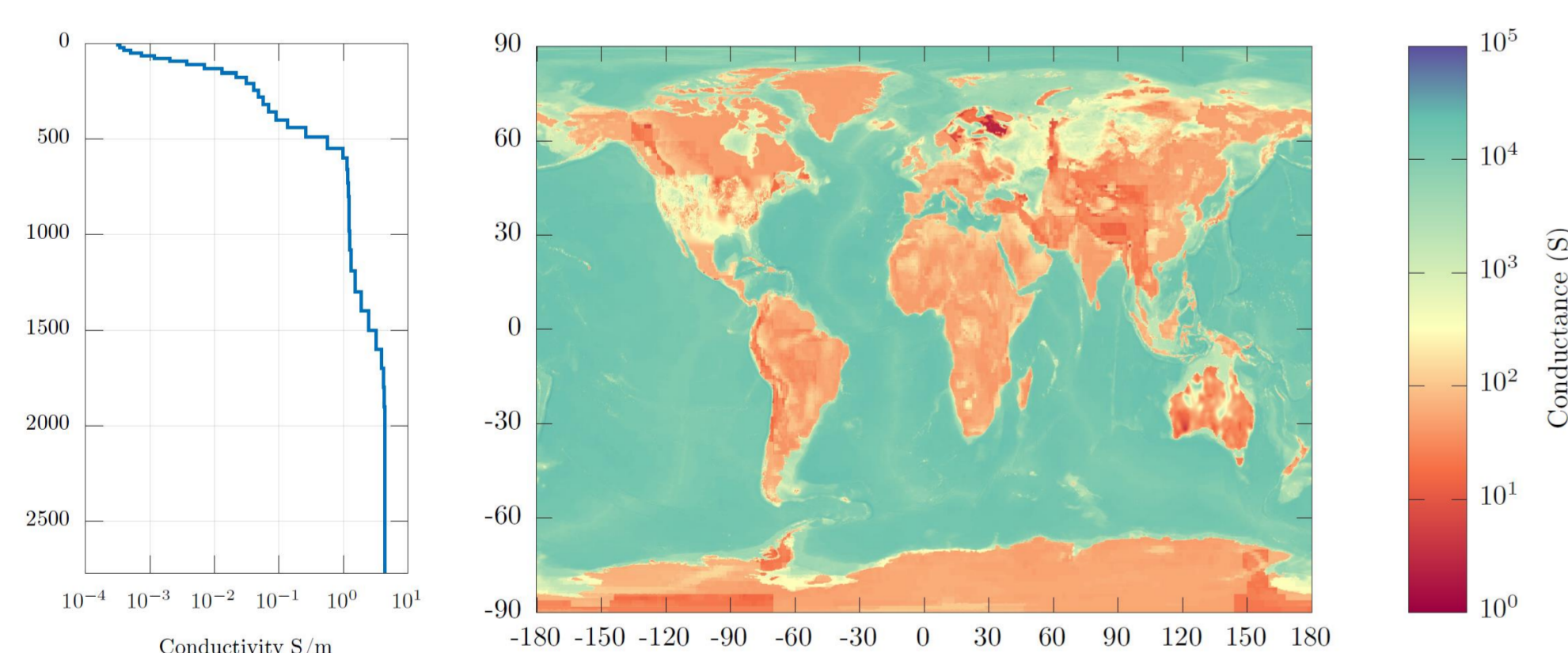


Fig. 1. Earth's conductivity model. Left: 1-D conductivity distribution beneath surface layer (from [8]). Right: 2-D conductance distribution in surface layer (from [6]).

4 Modelling (ionospheric) daily variations

We assume that DV are of ionospheric origin only. With some efforts, these signals can be written as

$$\mathbf{B}^{\text{iono,TIE}}(\mathbf{r}, t_k; \sigma) = \sum_{j=1}^{N_j} \sum_{n=0}^{N_p} e_j(t_k - n\Delta t) M_{\mathbf{B}_{j,p}}^n(\mathbf{r}, T; \sigma) \quad (2)$$

where N_j : number of spatial modes (SM) for each $p = (k - n) \bmod N_p$, $N_p = 24$, $M_{\mathbf{B}_{j,p}}^n$: time invariant weights; their calculation is discussed in Section 5, e_j : external expansion coefficients.

Superscript "TIE" means that parameterization of these signals relies on (physics-based) Thermosphere-Ionosphere-Electrodynamics General Circulation Model (TIEGCM; [9]) simulations. Note, that TIEGCM aims to describe PEJ, EEJ, and MLCS.

5 Implementation

- Step 1:** Take external radial magnetic field simulated by TIEGCM at 24x678 time instants at a grid of 2x5 degrees; 24 stands for 24 hours, 678 stands for number of days in two TIEGCM runs;
- Step 2:** Interpolate the field on a much denser grid;
- Step 3:** Calculate (external) stream function from the interpolated field;
- Step 4:** Perform PCA of stream function SH expansion for UT time instants $h=0, 2, \dots, 23$ [1]

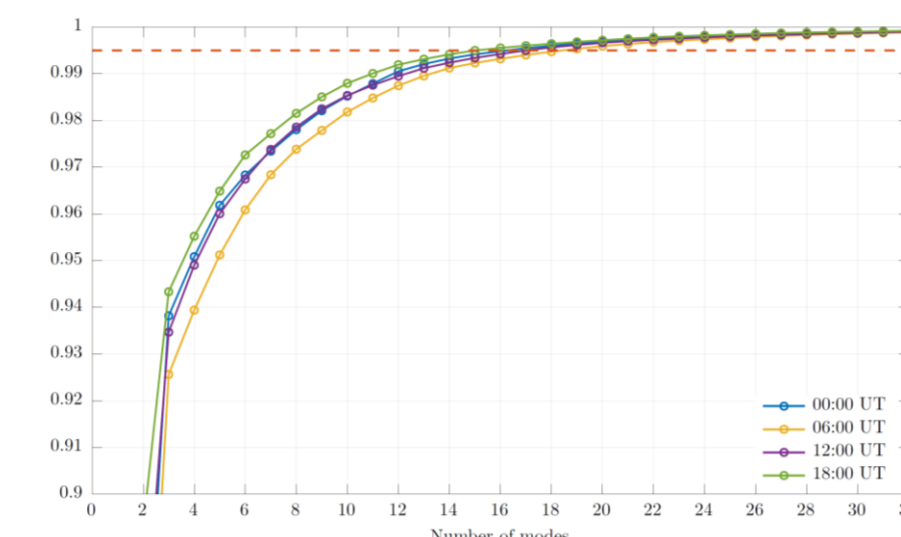


Fig. 2. Cumulative variance for the first 32 modes for the selected h (0, 6, 12, 18). The red dashed line marks the 99.5% threshold. The figure demonstrates that **16 modes** explain the spatial structure of TIEGCM-based stream function, irrespective of h .

- Step 5:** Calculate 24x16 external currents from 24x16 stream function spatial modes;
- Step 6:** Calculate magnetic fields $\mathbf{B}_{j,p}$ at 0.1x0.1 degrees grid excited by external currents from Step 5 in a given conductivity model (Fig. 1). Calculations are performed in frequency domain (using GEMMIE solver [5]) at periods from 1 to 10^7 hours;
- Step 7:** Calculate time-invariant weights $M_{\mathbf{B}_{j,p}}^n$ (eq. 2) using formalism from [6];
- Step 8:** Repeat Steps 6 and 7 but using $L(L+2)$ SH-based elementary currents [6] to calculate weights $M_{\mathbf{B}_l^m}^n$ (L is maximum degree in SH expansion in eq. 1);
- Step 9:** Take 1997-2021 hourly means of observatory magnetic field and subtract from them CHAOS [3] core and crustal fields;
- Step 10:** Perform least-square analysis (considering as modelled data the sum of left-hand sides in eqs (1)-(2) and as observed data the data from Step 9) to estimate \mathcal{E}_l^m and e_j at each time instant of 1998-2021 years; procedure is described in [6];

Incorporating estimated coefficients into eqs. (1)-(2) again, one can calculate magnetic field and actual external current at any time instant of 1998-2021 years, either on a grid or at observatory locations.

6 Results

We took in eq. (1) SH expansion up to degree $L=2$ [2], giving us $L(L+2)=8$ coefficients to estimate \mathcal{E}_l^m at each time instant. In eq. (2) we take $N_j=16$ (see Fig. 2). For comparison we performed the following experiment: we ignored eq. (2) and estimated coefficients \mathcal{E}_l^m only, but up to degree $L=4$ giving us $L(L+2)=24$ coefficients at each time instant. $L=4$ is chosen to have the same number of SM (8+16). The latter setup allows us to catch up magnetospheric and ionospheric (at least partly) contributions. The results are shown in Figs 3 - 6.

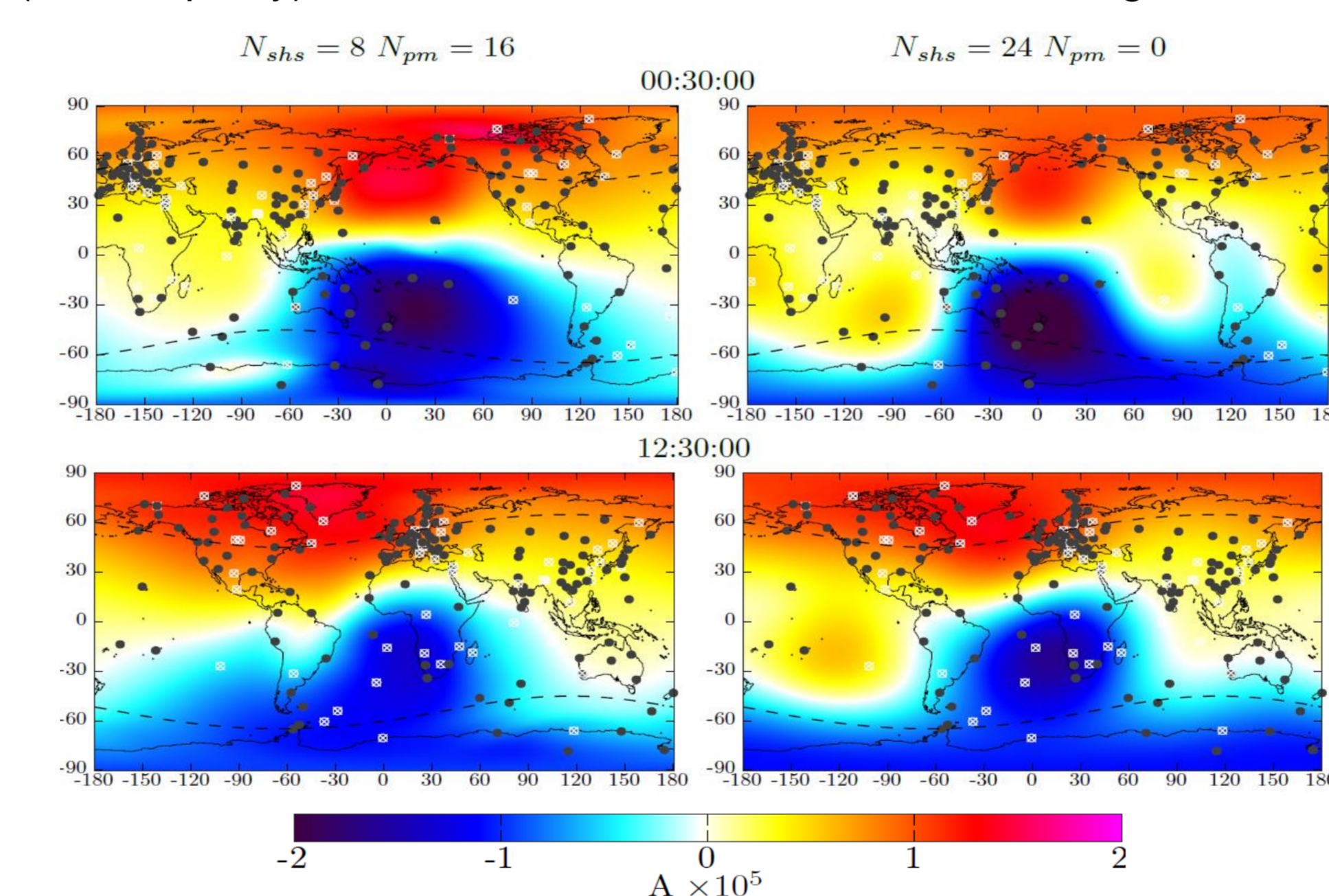


Fig. 3. Comparison of stream functions (for two setups, 8+16 and 24+0) at two quiet time instants (00:30 and 12:30 UT) of March 17 2009. Both magnetospheric (dominant first zonal harmonic structure) and ionospheric contributions (two whorls) are visible. Interestingly, "24+0" results show artefacts (?) to the left and to the right of two whorls. Also in "8+16" result, some structures in polar regions are noticeable. White circled crosses depict observatory at which the data were absent for these time instants.

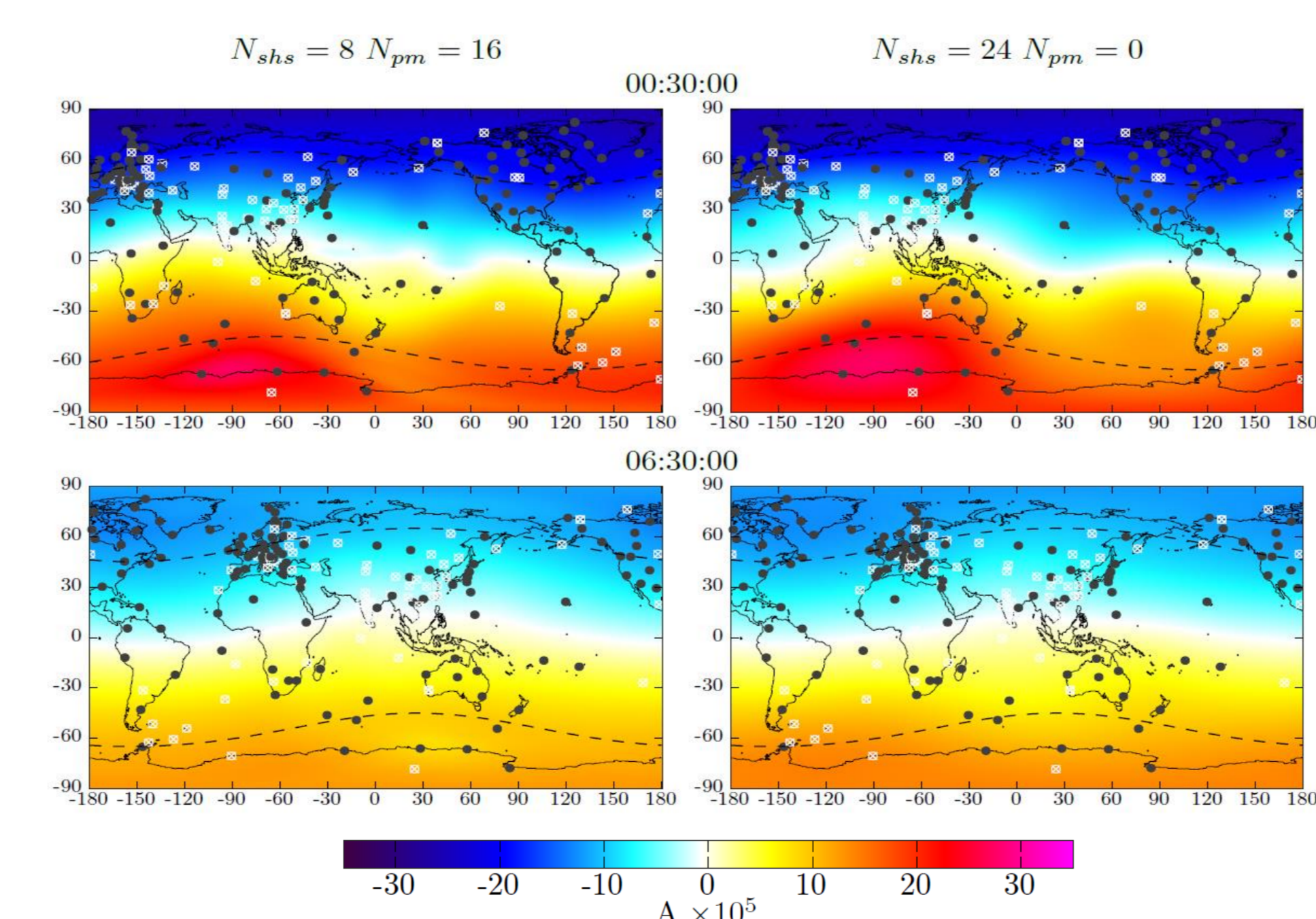


Fig. 4. Comparison of stream functions for two setups at two storm time instants of October 29 2003 (Halloween storm). Results for two setups are similar, indicating that SH expansion up to degree 2 is adequate to describe magnetospheric source, as also pointed out in [2]. We notice also different dynamic range of the signals in Figs 3 and 4.

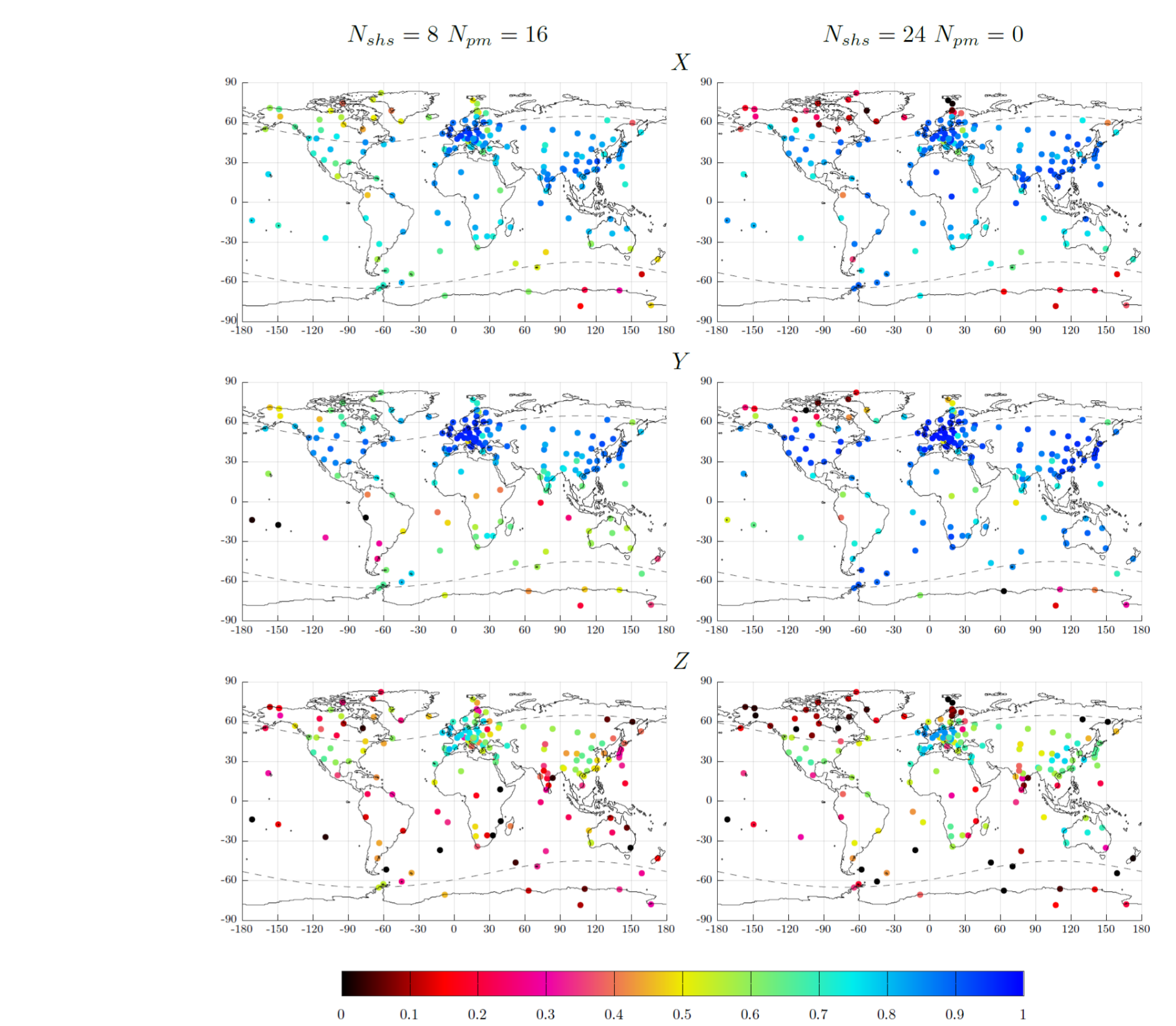


Fig. 5. Coefficient of determination R^2 for 1998-2021 time instants with $K_p < 2$ (for two setups described above). One can observe that: a) R^2 is significantly smaller in vertical component; b) R^2 is the largest in Y component; c) in all components R^2 is the largest in the regions with relatively dense grid of observations (Europe, China); d) R^2 is noticeably larger in polar regions for "8+16" setup; e) in non-polar regions R^2 is slightly larger for "24+0" setup. The latter may indicate that TIEGCM needs an improvement.

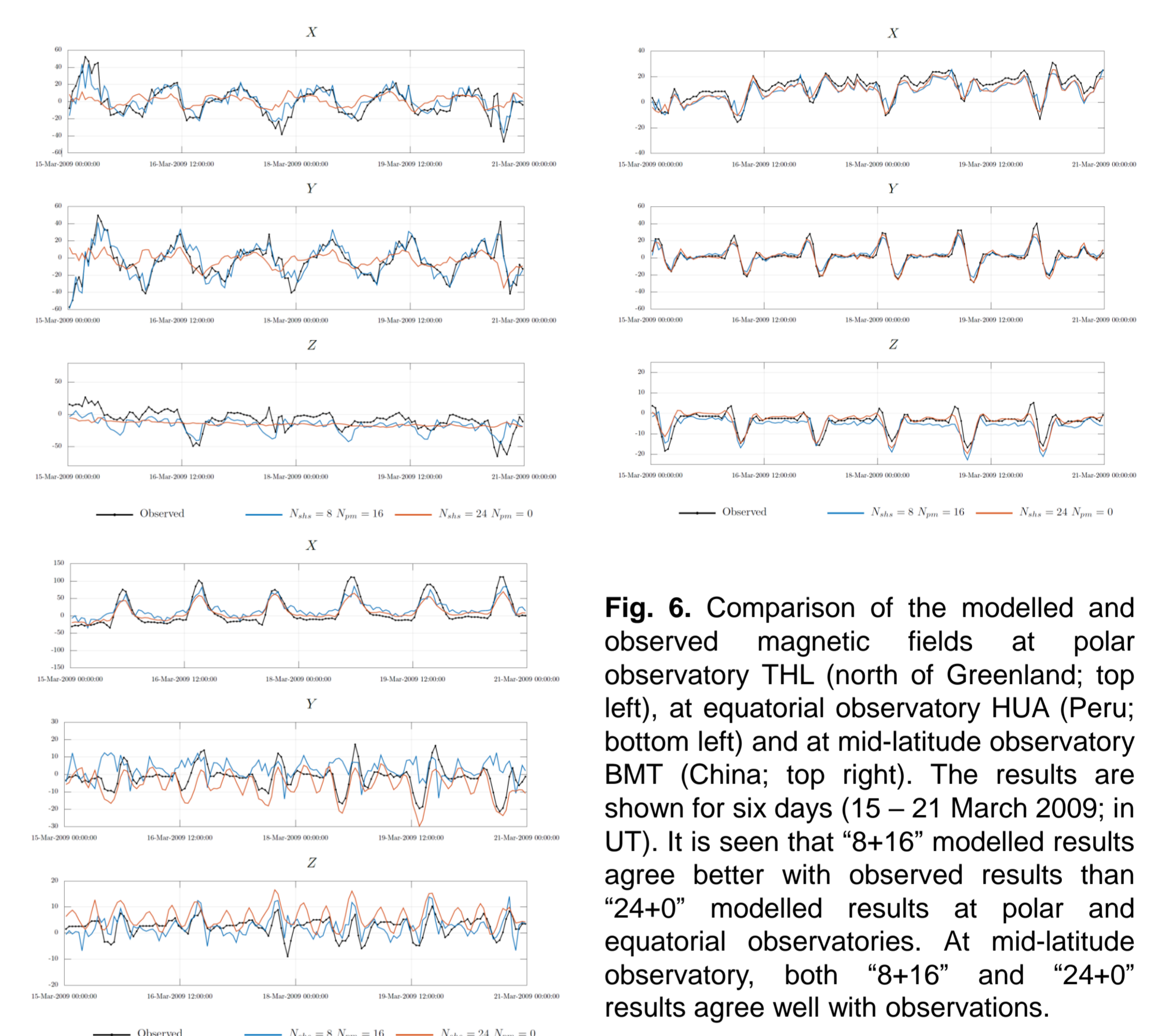


Fig. 6. Comparison of the modelled and observed magnetic fields at polar observatory THL (north of Greenland; top left), at equatorial observatory HUA (Peru; bottom left) and at mid-latitude observatory BMT (China; top right). The results are shown for six days (15 – 21 March 2009; in UT). It is seen that "8+16" modelled results agree better with observed results than "24+0" modelled results at polar and equatorial observatories. At mid-latitude observatory, both "8+16" and "24+0" results agree well with observations.

7 Concluding remarks

- We present a methodology for a joint modelling of magnetic field signals due to magnetospheric and ionospheric sources directly in time domain.
- We implemented the methodology for 24 years (1998-2021) of observatory data and show that the approach enables obtaining continuous spatio-temporal evolution of the magnetic field [7].

8 Outlook

Having \mathcal{E}_l^m and e_j estimated from observatory data, **one can then separate magnetospheric and ionospheric contributions in \mathcal{E}_l^m using satellite data** (assuming that corresponding ionospheric current flows in a thin layer below the satellite orbits).

Separation is possible because:

- Induced parts of $\mathbf{B}^{\text{mix,SH}}$ and $\mathbf{B}^{\text{iono,TIE}}$ are continuous across ionospheric layer and can be upward continued to satellite orbits;
- External part of $\mathbf{B}^{\text{iono,TIE}}$ has a jump across ionospheric layer but also can be upward continued to satellite orbits;
- External part of $\mathbf{B}^{\text{magn,SH}}$ is continuous across layer, but external part of $\mathbf{B}^{\text{iono,SH}}$ has a jump across it, meaning that radial dependence is different in corresponding external parts at satellite orbits;

Work is in progress to perform separation using *Swarm* and *MSS* data.

9 References

- [1] Alken, P., Maute, A., Richmond, A. D., Vanhamaki, H., Egbert, G. D., 2017. An application of principal component analysis to the interpretation of ionospheric current systems. *Journal of Geophysical Research: Space Physics*, 122, 5687-5708, <https://doi.org/10.1002/2017JA024051>
- [2] Fillion, M., Chulliat, A., Alken, P., Kruglyakov, M., & Kuvshinov, A., N. Schnepf, 2023. A model of hourly variations of the near-Earth magnetic field generated in the inner magnetosphere and its induced counterpart. *J. Geophys. Res.*, 128, e2023JA031913, <https://doi.org/10.1029/2023JA031913>
- [3] Finlay, C., Kloss, C., Olsen, N., Hammer, M., Toffner-Clausen, L., Grayver, A., Kuvshinov, A., 2020. The CHAOS-7 geomagnetic field model and observed changes in the South Atlantic Anomaly. *Earth, Planets and Space*, 72, 1562-1572, <https://doi.org/10.1186/s40623-020-01252-9>
- [4] Kuvshinov, A., Manoj, C., Olsen, N., Sabaka, T., 2007. On induction effects of geomagnetic daily variations from equatorial electrojet and solar quiet sources at low and middle latitudes. *J. Geophys. Res.*, 112, B10102, [doi:10.1029/2007JB004955](https://doi.org/10.1029/2007JB004955)
- [5] Kruglyakov, M., Kuvshinov, A., 2022. Modelling tippers on a sphere. *Geophys. J. Int.*, 231(2), 737-748, <https://doi.org/10.1093/gji/ggac199>
- [6] Kruglyakov, M., Kuvshinov, A., Nair, M., 2022. A proper use of the adjacent land-based observatory magnetic field data to account for the geomagnetic disturbances during offshore directional drilling. *Space Weather*, <https://doi.org/10.1029/2022SW003238>
- [7] Kruglyakov, M., Kuvshinov, A., 2024. Joint time-domain modelling magnetic field variations of ionospheric and magnetospheric origin. A concept and implementation to observatory data, in preparation.
- [8] Kuvshinov, A., Grayver, A., Toffner-Clausen, L., Olsen, N., 2021. Probing 3-D electrical conductivity of the mantle using 6 years of *Swarm*, *CryoSat-2* and observatory magnetic data and exploiting matrix Q-responses approach. *Earth, Planets and Space*, 73, <https://doi.org/10.1186/s40623-020-01341-9>
- [9] Maute, A., 2017. Thermosphere-Ionosphere-Electrodynamics General Circulation Model for the Ionospheric Connection Explorer: TIEGCM-ICON. *Space Science Reviews*, 212 (1-2), 523-551.